DEMONSTRATION OF A MICROFABRICATED HIGH-SPEED TURBINE SUPPORTED ON GAS BEARINGS

Luc G. Fréchette, Stuart A. Jacobson, Kenneth S. Breuer[1], Fredric F. Ehrich, Reza Ghodssi[2], Ravi Khanna, Chee Wei Wong, Xin Zhang, Martin A. Schmidt and Alan H. Epstein

Gas Turbine Laboratory and Microsystems Technology Laboratories
Massachusetts Institute of Technology
Cambridge, MA 02139

ABSTRACT

A single-crystal silicon air turbine supported on gas lubricated bearings has been operated in a controlled and sustained manner at rotational speeds greater then 1 million rpm and power levels approaching 5 W. The device is a second-generation version of the microbearing rig first reported by Lin *et al*. [1], and is the first micromachine to operate at circumferential tip speeds of hundreds of meters per second, comparable to conventional scale turbomachinery. To achieve this level of peripheral speed, microfabricated rotors must withstand large induced stresses, need a sufficient power source to drive them, and require stable, low friction bearings for support. This paper focuses on process improvements in the microbearing device fabrication and on the advances in operating micro-gas bearings and micro-turbomachinery. The successful operation of this device motivates the use of this technology for high-power density MEMS.

INTRODUCTION

To achieve high power and efficiency from a rotating device, high circumferential tip speed is a necessity. Conventional scale turbomachinery typically run with tip speeds of order 500 m/s, enabling high-power density applications such as gas turbines for aircraft propulsion and power generation. In order to achieve high levels of power density, microfabricated rotors will need to run at comparable tip speeds. Typical rotating micromachines, such as gears and micromotors, are formed either by surface micromachining or LIGA, supported by solid contact on a pin bearing, and entrained by electrical or contact forces acting on the edges of the rotor. These micro-rotors have reached of order 2 m/s tip speed [2], which is two orders of magnitude lower than desired for Power MEMS applications.

An effort was undertaken at MIT to develop high-speed rotating devices to enable high-power density MEMS [3]. In the current approach, the rotor is etched from the bulk substrate, taking advantage of the high strength-to-density ratio of single crystal silicon. Fluid film lubrication supports the rotor, reducing the resistance to rotation and preventing wear due to solid contact. Micro-turbomachinery is used as a drive source for high-power density fluid-to-mechanical energy conversion. In order to demonstrate this approach and develop the requisite technology, a microturbine-driven bearing rig was developed. This paper presents the design, fabrication, and operational achievements since the previously reported results of Lin *et al*. [1].

DEVICE DESIGN AND DESCRIPTION

The microbearing device, shown in Figures 1 and 2, consists of a 4.2 mm diameter rotor enclosed in a fusion-bonded stack of five aligned, through-etched wafers. The rotor is a planar disk with radial turbine blades on its front side. Pressurized air enters the device near the outer edge and flows radially inward, first through a set of stationary (stator) vanes and then through the rotor blades, exhausting axially near the center of the device. A gas bearing on the periphery of the rotor supports radial motion, while a pair of gas thrust bearings on the device centerline supports axial motion. The stator vanes, shown in Figure 3, are curved, turning the flow away from purely radial, imparting angular momentum to the flow as it accelerates. The turbine rotor blades turn the flow back toward radial, extracting angular momentum in the process. The angular momentum change across the rotor produces a torque. The power transferred to the rotor is the product of this torque and the rotor's angular rotation rate. For this application, the turbine was designed to provide sufficient power to overcome the viscous drag in the bearings and on the back side of the rotor, which goes like the square of the rotation rate. The total drag is approximately 13 W at a circumferential tip speed of 500 m/s. While viscous drag is relatively large in microsystems due to the small length scale [4], it is still quite small compared to the capabilities of high-speed turbomachinery. The turbine for this device had to be intentionally designed to match the relatively low power requirements of the viscous drag. Alternative turbine designs, compatible with the current process and geometric constraints, that produce tens of watts of power (beyond the drag requirements) have been designed for Power MEMS applications.

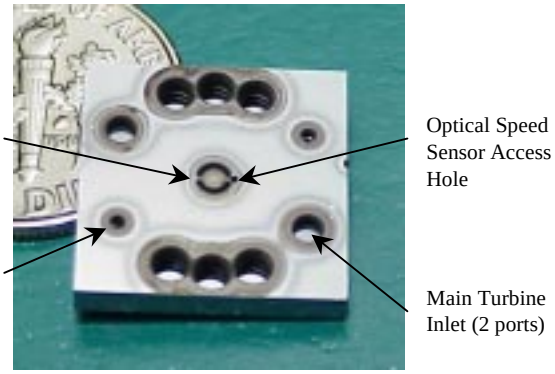

Figure 1. *Microturbine-driven bearing rig die, consisting of a diced five-wafer bonded stack, which encloses a 4.2 mm rotor.*

[1] Present Address: Brown University, Division of Engineering

[2] Present Address: University of Maryland, Department of Electrical and Computer Engineering

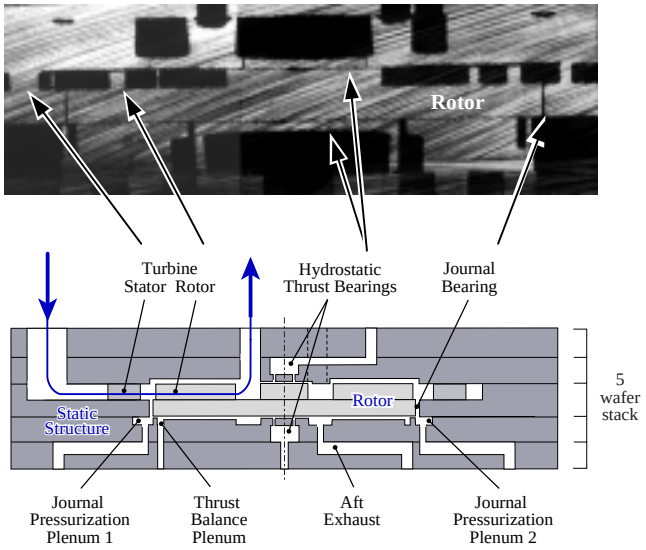

Figure 2. *Optical photograph (top) and schematic (bottom) of a cross-section of the microturbine-driven bearing rig.*

The turbomachinery was designed using MISES, a two-dimensional computational fluid dynamics code developed at MIT [5]. MISES is an Euler solver coupled to an integral boundary layer formulation. The actual flow through the turbine is expected to be three-dimensional, mainly due to boundary layer growth on the end-walls. However, because the turbine flow is accelerating, the three-dimensional effects are not expected to be substantial [6]. The particular challenge in the design of microturbomachinery for MEMS results from the microfabrication constraint that limits us to constant blade height. A more traditional design for centrifugal turbomachinery would allow the blade height to vary inversely with radius to compensate for the increase in circumference with radius. The resulting blade designs reflect the different strategies that a designer must use to adjust for the differences in fabrication capability.

The hydrostatic gas thrust bearings were demonstrated in the first generation of this device [1]. The hydrostatic gas journal bearing, which supports radial motion, is new to this device. The journal bearing, formed in the gap between the rotor and the stator at the periphery of the rotor, acts as a radial spring. The journal bearing is 300 μm deep and has an average width of 15 μm with the rotor centered. A pressure differential is maintained across the journal bearing, generating an axial through flow. On the front side of the rotor, the journal bearing boundary pressure is set by the stator exit/rotor inlet pressure, called the interrow pressure. On the back side of the rotor, the journal bearing opens into a large plenum whose pressure can be set externally. The current implementation splits the back side plenum into two symmetric journal pressurization plenums, as shown in Figure 2, although for current testing these two plenums are typically set to the same pressure.

The pressure supplied to the journal pressurization plenums is maintained higher than the interrow pressure so that there is an axial flow across the journal bearing from the back side to the front side. As the flow goes through the journal bearing gap, there is a pressure drop associated with entering the bearing, with the development of the boundary layer in the gap, with flow through the bearing from viscous effects, and finally with exiting the bearing. Each of these losses can be viewed as a resistance, and several of these resistances are functions of the local journal bearing width. When the rotor moves off center so that the journal

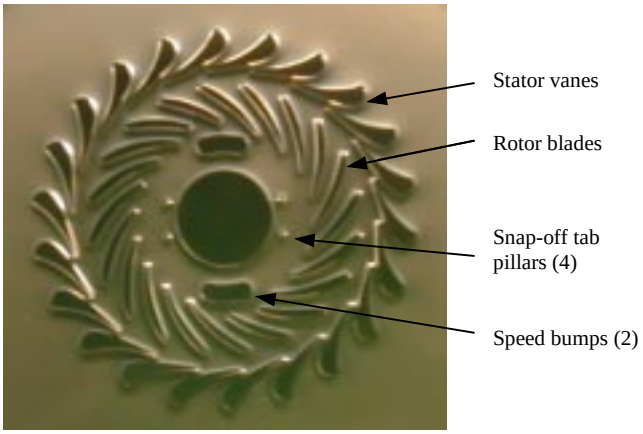

Figure 3. *SEM of the 4.2 mm diameter microturbine showing the 150 μm tall stator and rotor blades, two symmetric speed bumps, and four pillars for the snap-off tabs. In this picture, the journal bearing gap remains to be etched.*

bearing width is smaller on one side than the other, the resistances on each side of the rotor result in axial pressure profiles through the journal bearing with differing distributions. When the pressure is integrated across and around the journal bearing, the resultant force on the rotor is a restoring one, in the direction to re-center the rotor. This hydrostatic bearing scheme was first demonstrated by Orr on a scaled-up bearing rig of similar geometry [7].

In addition to the two journal pressurization plenums for the journal bearing, there is a circumferential plenum on the back side of the device, referred to in Figure 2 as the thrust balance plenum. While there is no stiffness associated with this plenum, it is used to help balance axial thrust on the rotor. The thrust balance plenum can be coupled to pressures elsewhere in the system, allowing the operator to compensate for axial loads on the rotor that develop as the pressure across the turbine is increased. In this way, the thrust balance plenum complements the thrust bearings.

Speed is measured with a fiber optic sensor that detects the passage of two diametrically opposite features on the silicon rotor. These two features, referred to as speed bumps in Figure 3, are at the same level as the blades and the thrust bearing hub, and are located on the rotor in the exhaust flow from the turbine. A fiber optic displacement measurement system is located above the speed bumps. With the rotor spinning, the output from this sensor approximates a low duty cycle square wave with frequency twice that of the rotor rotation rate.

FABRICATION

The fabrication process is based on deep reactive ion etching (DRIE) and aligned fusion-bonding of five silicon wafers to create fluidic interconnects and enclose the rotor. An exploded view of the five-wafer stack device is shown in Figure 4. The process flow was first presented by Lin *et al.* [1] and remains the foundation for this second generation device. This section summarizes the fabrication sequence, describes photolithography development necessary for precision high-aspect ratio DRIE, and presents a new rotor release strategy.

The end plates (wafers 2 and 4) first receive shallow silicon etches on their side facing the rotor. All the wafers are then deep etched halfway through their thickness, except for wafer 1, which

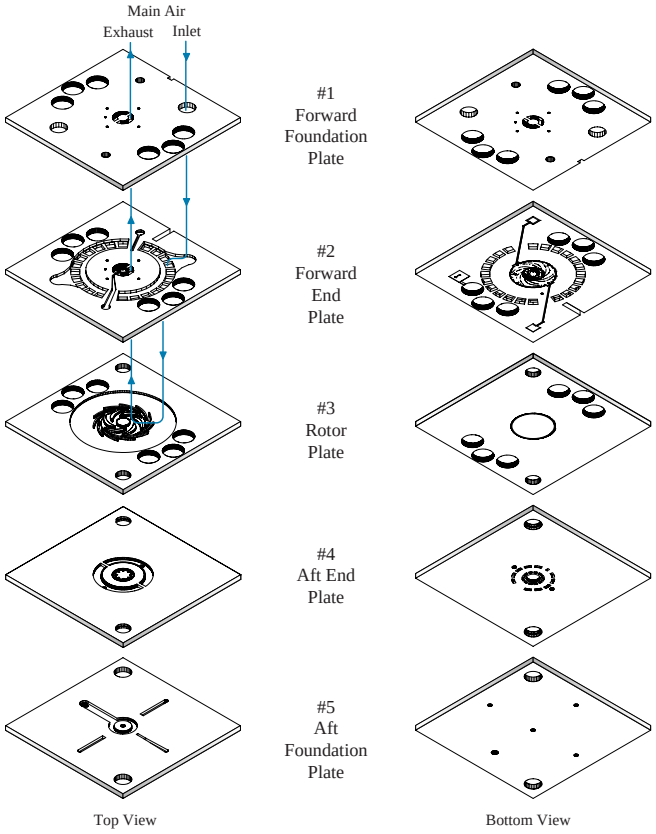

Figure 4. *Top and bottom view of the five-stack device. The die is 15 mm per side and 2.3 mm thick.*

is etched through from its bottom side. Wafers 2, 4 and 5 are then deep etched on the opposite side until through-flow channels are created. Wafer 3 is then bonded to wafer 2 and etched from the bottom side to define the journal bearing gap. Finally, wafers 1, 4, and 5 are fusion-bonded to wafers 2 and 3 in a single step.

During through etching, the wafers are reversibly mounted to a quartz substrate to prevent leakage of He coolant when the etch breaks through. The bonding surface on the back side of wafers are protected to prevent deposition of hydrocarbon residue from the DRIE passivation step [8] and damage from ion back-scattering off of the quartz handle wafer. For the die shown in Figure 1, the back of wafer 1 was not protected during its through etch from the bottom side, and the resulting surface contamination can be seen around the holes.

The required level of accuracy for the micromachined geometries is driven by their functionality. The two outermost wafers provide external fluidic and optical ports to the die, resulting in dimensions of the order of hundreds of microns without stringent precision requirements. Moving inwards toward the rotor, the end plates (wafers 2 and 4) feature pressurized plenums (on their outer side) and 10 μm diameter by 100 μm long orifices for the thrust bearings (on their side facing the rotor). Accurate dimensions are critical since the axial stiffness of the thrust bearing depends on the pressure drop across the orifice, which is a strong function of its diameter. Orifices with a diameter of 10-11 μm were reproducibly achieved by exposing a 7 μm diameter circle through a 6 μm thick resist (AZ4620). The optimized process resulted in an 8-9 μm diameter opening in the resist, and 1 μm of blowout in the silicon after 90 minutes of DRIE. The rotor is cut from the back of

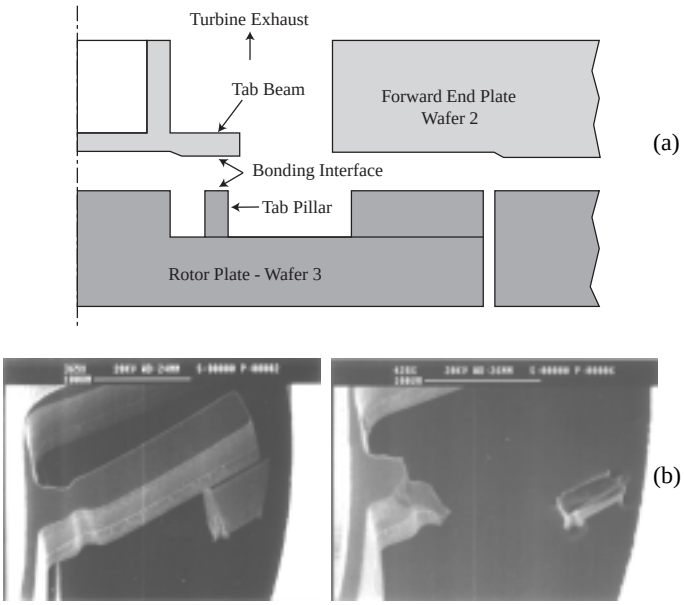

Figure 5*. (a) Schematic of snap-off tab configuration. (b) SEM of bonded snap-off tab structures before and after fracture.*

the center wafer by a high-aspect ratio circumferential trench, which simultaneously creates the journal bearing geometry. From an initial 4 μm line width in the mask, a final DRIE trench tapering from 17 to 9 μm wide and 300 μm deep was achieved using a 10 μm thick photoresist. In both processes, the minimum feature size consistently achievable was limited by the trade-off between the photoresist thickness necessary to withstand the etch duration, the increase in etch duration for smaller features, and the lower selectivity of DRIE recipes with less lateral etch.

An on-going challenge in the fabrication of micro-rotors is a reliable process flow to create free parts within enclosed structures, without tedious manual assembly and risk of damage. The approach adopted consists of bonding wafers 2 and 3 before the journal is etched, creating silicon tabs which connects the rotor to the adjacent wafer, similar to the approach presented by Lin *et al.* [1]. As shown in Figure 5(a), a silicon pillar extending from the rotor bonds to a horizontal beam on the forward end plate. The journal bearing is then etched and the remaining three wafers are aligned fusion bonded to complete the five-stack. The silicon links are then mechanically fractured to release the rotor before testing, acting as *snap-off tabs*. This differs from Lin *et al.*, who used a laser assisted etch to remove the tabs. The tab geometry was designed to provide a solid support against axial and in-plane motion of the rotor, while allowing a controlled failure mode upon lateral force. An array of configurations were designed using simple beam theory and stress concentration relations, and tested aiming for a clean fracture at the roots of the pillar and beam. Micromachined silicon needles were specially designed to reach down the main exhaust port and apply the necessary lateral force to snap the tabs. Figure 5(b) shows such a snap-off tab structure before and after being fractured. The fractured surfaces are raised from the disk surface, which is important so as not to introduce stress concentrations. These snap-off tabs have been successfully used in two five-stack builds. Particles generated during snap-off were removed by blowing nitrogen through the main turbine flow path, out the main exhaust.

EXPERIMENTAL DETAILS

The microturbine-driven bearing rig die mounts in an acrylic package using o-rings to create sealed fluidic connections to the die. Plastic tubing connects the package to a gas handling system, which includes a high-pressure nitrogen source, valves to distribute pressures to the various ports, pressure sensors, mass flow meters, a PC-based data acquisition system, and a fiber optic speed sensor.

During operation, the signal from the speed sensor is monitored on a spectrum analyzer. The spectrum analyzer shows a strong peak at twice the rotation rate (two speed bumps per rotation), at the rotation rate due to asymmetry, and also at higher harmonics. Under certain conditions, extra peaks also appear, as shown in Figure 6. These peaks are evidence of excitation of the bearing natural frequency. As mentioned earlier, the hydrostatic journal bearing acts like a spring, and as such has a natural frequency associated with it. Whirling of the rotor at the natural frequency of the bearing results in precession of the speed bumps, which appears as a pulse width modulation of the signal at the whirl frequency. The measured interaction between the rotation rate and the bearing natural frequency also results in peaks at their combinations, as identified in Figure 6. Operation has shown that appearance of these extra peaks is associated with the approach of a stability boundary. The differential pressure across the bearing can usually be adjusted to stabilize the rotor and make these peaks vanish. The ability of the speed sensor to pick up this additional information has been an important diagnostic tool.

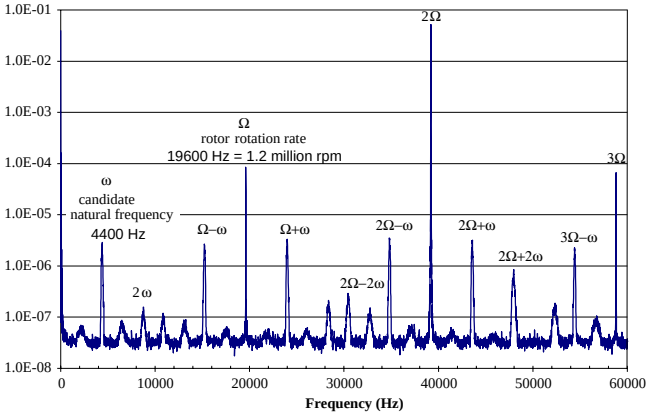

***Figure 6**. Power spectrum of the optical speed sensor signal showing the speed bump frequency (2Ω) and the rotor rotation rate (Ω), as well as other peaks corresponding to the natural frequency (ω) and its combinations with the rotation frequency.*

Figure 7 shows the rotation rate of two devices as they are slowly accelerated in a stable manner. As the turbine supply pressure increases, the pressures applied to the hydrostatic journal bearing are also increased according to a predetermined schedule. Device 1 was brought up to a tip speed of 260 m/s (1.2 million rpm) and was held there for 20 minutes (a pressure leak resulted in a slight deceleration). The rotor was then rapidly decelerated to stop. Device 2 reached a tip speed of 303 m/s (1.4 million rpm) prior to going unstable and crashing. Both devices achieved of order 10^8 revolutions. The operating schedule is one suspect in the cause of the crash of Device 2. More dies are currently being tested to help map out safe areas of operation. Four other dies from this build have already been tested, but they have only been able to reach tens of thousands of rpm prior to instability. The main problem limiting high-speed operation is believed to be rotor imbalance. Balance is limited by our ability to align masks on the front and back side of the rotor wafer, and by the uniformity of the blade etches across a rotor. When the bearing operates at rotation rates higher then the journal bearing natural frequency (supercritically), as it does through most of its operating range, the rotor spins around its center of mass rather than its geometric center. This offset of the rotor produces circumferential pumping of fluid, causing the development of hydrodynamic forces in the journal bearing gap. These hydrodynamic forces are relatively small if the imbalance is small, but they increase with the square of speed. The hydrodynamic forces tend to be destabilizing [9].

Figure 8 shows the turbine operating line for Devices 1 and 2. These operating lines are comparable in shape to those observed for macroscale turbines. Also shown in this figure are three data points calculated using MISES with the corresponding power delivered by the microturbine. At 1.4 million rpm, the microturbine is predicted to deliver nearly 5 W of mechanical power with a torque of over 30 μN-m. The computational results are dependent on the axial position of the rotor, which affects the amount of drag. The uncertainty bars on the MISES data points are associated with an expected +/- 0.5 μm uncertainty in the axial position of the rotor. The MISES results do not compensate for the decrease in mass flow due to blockage from boundary layer growth on the end-walls

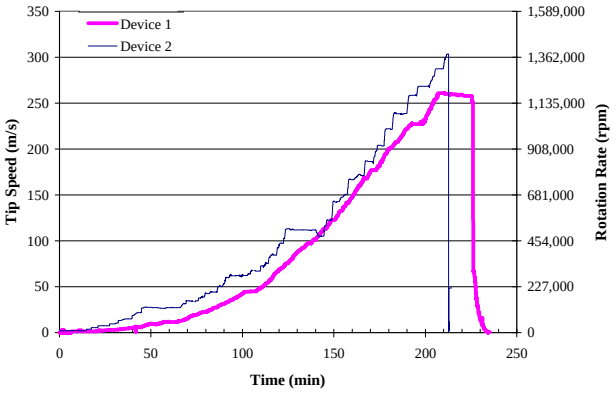

***Figure 7**. Speed evolution over time. Uncertainty in the tip speed measurement is ±0.5% of the measured speed.*

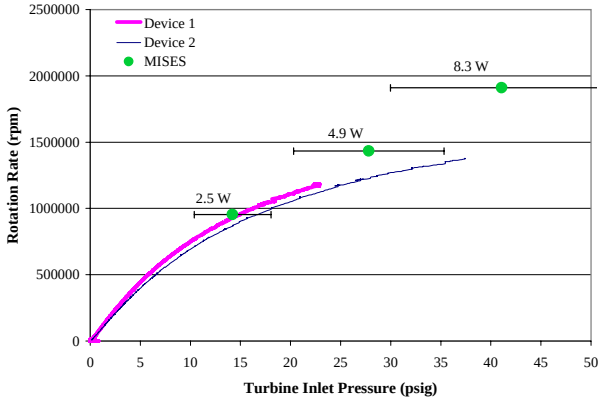

***Figure 8**. - Rotation rate as a function of the air pressure supplied to the turbine. There is a ±0.8 psi uncertainty in the pressure.*

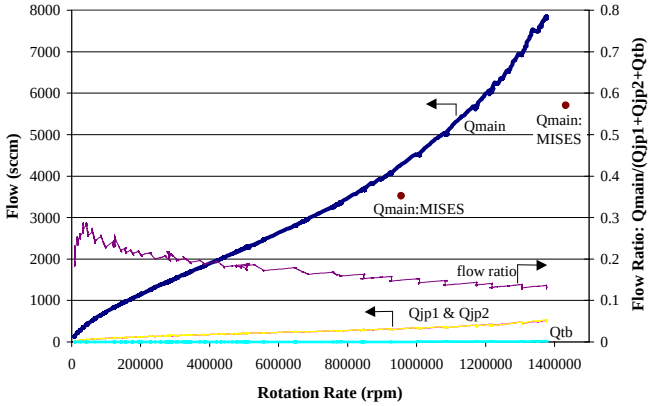

Figure 9. *Turbine and bearing flow rates over the range of operating speeds for Device 2. Uncertainty in the main flow is ±200 sccm, in the journal pressurization plenums (jp1 & jp2) is ±50 sccm, and in the thrust balance plenum (tb) is ±0.5 sccm.*

(three-dimensional effect), which likely explains why the actual device required a somewhat higher turbine pressure for a given speed to generate sufficient torque. At 1.4 million rpm, the differential pressure across the journal bearing was about 5 psi.

The mass flow rates supplied to Device 2 are shown in Figure 9. Here the experimental turbine flow rate (Qmain) is somewhat higher than predicted in MISES, due to the increased pressure required to operate the turbine. The flow rates supplied to each journal pressurization plenum (Qjp1 and Qjp2) are essentially equal, lying on top of each other in Figure 9. The thrust balance plenum was sealed with negligible leakage. Also shown in Figure 9 is an aggregate of the back plenum flows normalized by the main turbine flow. This ratio peaks at a value of 0.3 at low speed, but decreases to 0.13 at the highest speed and is still trending down. Thus, for high-speed applications, the flow needed to operate the hydrostatic journal bearing is small compared to the main turbine flow.

The thrust bearings proved sufficiently stiff so as not to require much manipulation during a run. For Device 2, the back side thrust bearing ran with a constant supply pressure of 35 psig while the front side thrust bearing was varied from about 60 – 85 psig. Each thrust bearing required about 10 sccm of nitrogen, which is negligible in the scale of the other flow rates (Figure 9).

CONCLUSIONS

A 4.2 mm diameter silicon rotor has been spun in a sustained manner at high speed using gas lubricated bearings. These microturbines have reached tip speeds of 300 m/s, corresponding to rotation rates of 1.4 million rpm. At this speed, the turbine provides nearly 5 W of power and achieves a power density greater than 4,000 MW/m^3 (based on turbomachinery volume), which is more than twice that achieved by modern aircraft engine turbine technology. This high level of power density is a direct benefit of the reduced length scale [4]. We are currently trying to understand more fully the stability characteristics of micro-gas bearings, with the goal of achieving self-sustained operation. Our fabrication effort is focusing on improving alignment precision and etch uniformity, to decrease the rotor imbalance. We believe this technology will serve as a building block for a wide array of high-power density MEMS devices, including pumps, compressors, heat engines and coolers.

ACKNOWLEDGEMENTS

This work is the result of a collective effort by the MIT microengine team. The authors would like to specifically thank Dr. A. Ayon for his guidance in deep reactive ion etching and wafer bonding techniques, Dr. C.C. Lin for his pioneering work in microturbine fabrication and testing, and for having suggested the snap-off tab approach, as well as Dr. E. Piekos, Dr. D. J. Orr, and the entire MIT microengine team. This work was supported by the Army Research Office (DAAH04-95-1-0093) under Dr. R. Paur and by DARPA (DAAG55-98-1-0365, DABT63-98-C-0004) under Dr. R. Nowack and Dr. J. McMichael, respectively.

REFERENCES

1. C.-C. Lin, R. Ghodssi, A. A. Ayon, D. Z. Chen, S. A. Jacobson, K. S. Breuer, A. H. Epstein, and M. A. Schmidt, "Fabrication and Characterization of a Micro Turbine / Bearing Rig," *in Proc. 13th IEEE Workshop on Micro Electro Mechanical Systems, MEMS'99*, Orlando, FL, Jan. 1999.

2. J. J. Sniegowski, S. L. Miller, G. F. LaVigne, M. S. Rodgers, and P. J. McWhorter, "Monolithic Geared-Mechanisms Driven by a Polysilicon Surface-Micromachined On-Chip Electrostatic Microengine", *Proc. Solid-State Sensors and Actuators Workshop*, Hilton Head Is., SC, June 2-6, 1996, pp. 178-182.

3. A. H. Epstein *et al*., "Micro-Heat Engine, Gas Turbine, and Rocket Engines – The MIT Microengine Project", AIAA 97-1773, *28th AIAA Fluid Dynamics Conference*, Snowmass Village, CO, June 1997.

4. S. A. Jacobson, "Aerothermal Challenges in the Design of a Microfabricated Gas Turbine Engine," AIAA 98-2445, 29th Fluid Dynamics Conference, Albuquerque, NM, June 1998.

5. M. Drela and H. Youngren, "MISES 2.1," MIT Computational Aerospace Sciences Laboratory, June 1995.

6. A. Mehra, "Computational Investigation and Design of Low Reynolds Number Micro-Turbomachinery," SM Thesis, Massachusetts Institute of Technology, 1997.

7. D. J. Orr, "Macro-scale Investigation of High Speed Gas Bearings for MEMS devices," Ph.D. Thesis, Massachusetts Institute of Technology, 1999.

8. A. A. Ayón *et al.*, "Characterization of a Time Multiplexed Inductively Coupled Plasma Etcher," *J. Electrochemical Society*, Vol. 146, No. 1, Jan 1999, pp. 339-349.

9. E. S. Piekos, D. J. Orr, S. A. Jacobson, F. F. Ehrich, and K. S. Breuer, "Design and Analysis of Microfabricated High Speed Gas Journal Bearings", *28th AIAA Fluid Dynamics Conference*, 1997, AIAA paper 97-1966.